JOURNAL OF COLLOID AND INTERFACE SCIENCE 175, 36–45 (1995)

Influence of the Surface Viscosity on the Hydrodynamic Resistance and Surface Diffusivity of a Large Brownian Particle

KRASSIMIR DANOV,* RICHARD AUST,†[1] FRANZ DURST,† AND ULRICH LANGE†

*Laboratory of Thermodynamics and Physico-Chemical Hydrodynamics, Faculty of Chemistry, University of Sofia, J. Bourchier Ave. 1, Sofia 1126, Bulgaria; and †Lehrstuhl für Strömungsmechanik, Universität Erlangen-Nürnberg, Cauerstrasse 4, D-91058 Erlangen, Germany

Received September 6, 1994; accepted March 2, 1995

The present paper treats the problem of the slow motion of a spherical particle, partially immersed in a viscous liquid. It relates to the theory of Brenner and Leal concerning the surface diffusivity of a large Brownian particle and provides important basic information on the so-called "drag-out problem." The numerical investigation yields the local velocity and pressure distribution, the hydrodynamic resistance, and the surface diffusion coefficient. The computations are carried out for low Reynolds and capillary numbers considering a stationary floating macroparticle on a viscous liquid–gas interface. Results are presented for different values of surface dilatational and shear viscosity and contact angles. Brownian motion of the particle is taken into account by integrating the resultant second-order partial differential equations with an alternating direct implicit method. The numerical results reveal for all contact angles a strong decrease of the surface diffusion coefficient when the surface viscosity increases. © 1995 Academic Press, Inc.

Key Words: drag force; torque; Brownian spherical particle; surface viscosity effect; hydrodynamic resistance; surface diffusivity.

1. INTRODUCTION

Almost 90 years ago Einstein (1) obtained a formula for the diffusion coefficient for solid spheres in the dilute limit in his classic paper "Eine neue Bestimmung der Moleküldimensionen." This relation was later generalized by Kubo (2) for cases with more complicated hydrodynamics, considering hydrodynamic resistance. These works have been put forward by many researchers, see the review in (3, 4). The theory of Einstein was extended by Brenner and Leal (5, 6) for the diffusion of surfactant molecules, modeled as noninteracting Brownian spheres at the interface between two immiscible fluids. The calculation of the surface diffusivity of these spheres has been reduced to an expression completely analogous to the corresponding bulk diffusion coefficient formula. In (7) the diffusion and resistance coefficients of macroparticles floating on a liquid–gas interface were treated from the viewpoint of Einstein's theory and the reciprocal theorem. Good agreement with the experimental data for the movement of polymer (melanin) particles on a surfactant free water–air interface was shown in this paper. The effect of surfactants on the Brownian motion was discussed in (8) and a formula for the surface diffusion coefficient was proposed in (9). Another viewpoint of these problems was discussed in (10) in order to interpret experimental measurements of the surface diffusion motion. Information on the diffusion coefficient, the dilatational elasticity, and the viscosity of a surface layer was provided. A simple Kelvin–Voight model, in which the elastic and viscous stresses are additive, was assumed for the material behavior of the layer during dilatational deformation. The results in (8–10) showed that the reduced mobility of the particle results in lowering the surface diffusivity. The surface diffusion coefficient is directly proportional to the surface diffusivity without surfactants and inversely proportional to the hydrodynamic resistance of the individual sphere. This is why an accurate determination of the hydrodynamic resistance of a spherical particle partially immersed in a viscous liquid layer is one of the more important problems of hydrodynamics.

Faxén (11) developed the method of reflection for a sphere moving between two parallel planes in a viscous fluid. A great deal of work was done in obtaining first- and higher-order wall corrections for particles in flows that are bounded by plane or cylindrical walls (12). However, the method mentioned above and the obtained solutions are not valid for arbitrary distances from the wall and when the particle is floating on a liquid–gas interface (13). Dean and O'Neill (14, 15) showed that the force and the torque acting on a spherical particle, which moves or rotates in a viscous fluid at an arbitrary distance from a plane parallel to the solid interface, can be accurately determined. The limiting behavior when the sphere is almost in contact with the wall was obtained rigorously in (16–18). An important step for understanding this problem was made by Yang and Leal (19), who presented analytical results for the motion of a viscous Newtonian fluid drop in the presence of a plane, deformable, interface in a velocity range where inertial effects may be neglected. Numerical solutions, obtained via the boundary–integral technique, were used in (20) to consider the effect

[1] To whom correspondence should be addressed.

0021-9797/95 $12.00

of a linear axisymmetric straining flow on the existence of steady-state configurations in which a neutrally buoyant spherical particle straddles a gas–liquid interface. The authors determined the critical capillary number, beyond which an initially captured particle is pulled from the interface by the flow, and its dependence on the equilibrium contact angle.

Most of the publications in this area are based on the hypotheses that the interface is nonviscous. When there are insoluble or soluble surfactants in the solution, the interface has a viscous behavior. Boussinesq (21) postulated the existence of a surface viscosity, conceived as the two-dimensional equivalent of the conventional three-dimensional viscosity possessed by bulk-fluid phases. Boussinesq's theory was generalized to material interfaces of arbitrary curvature in the papers of Sternling and Scriven (22, 23). The effects of bulk and interfacial rheological properties and surfactant adsorption–desorption kinetics on the rate of drainage of foam and emulsion films were studied in (24, 25). The strong influence of the surface viscosity on the drag and torque coefficients of a spherical particle close to the viscous interface and in the liquid layer, bounded by the viscous interfaces, when the radius of the particle is of the same order of magnitude as the thickness of the liquid film was discussed in (26, 27). The effect of Gibbs' elasticity and surface viscosity on the drag coefficient of an emulsion droplet in adsorption-controlled Marangoni flow was presented by Levich (28) and Edwards *et al.* (29). They showed that in this case only the dilatational surface viscosity influences the drag coefficient. The effect of Gibbs' elasticity is usually neglected when the concentration of insoluble surfactants is small, the diffusion of soluble surfactants is fast, or the concentration of soluble surfactants is greater than the critical micellar concentration. In these cases we can calculate the flow in the frame of Newtonian volume and surface rheology not taking into account the equations for the surfactants mass balance.

The general approach, along with some important technological and biological applications, is considered in several monographs (4, 29–32). Here we mention only some of them: the thin film coating, the drag-out problem, the material properties of the red blood cell membrane and its physiological functions (10), etc.

The present paper discusses the problem of determining the drag force and torque exerted on a solid particle floating on a viscous liquid–gas interface for low Reynolds and capillary numbers. The free surface-excess pressure tensor considers the Boussinesq (21) and Scriven (23) constitutive law for a Newtonian interface. It is proved in detail in Section 2 that the problem for Stokes' flow in a coordinate system of revolution with specific bicylindrical coordinates in the meridian planes can be reduced from three dimensions to two dimensions, which is convenient for numerical investigations. For viscous interfaces, the boundary conditions contain second-order derivatives of the velocity, for which no analytical solution is known. The diffusion coefficient for floating macroparticles is treated from the viewpoint of Einstein's theory of diffusion. In order to illustrate the strong influence of the surface viscosity on the hydrodynamic resistance and the dependence of the surface diffusion coefficient on the equilibrium contact angle, the drag and the torque coefficients, the velocity and the pressure distribution are presented in Section 3. The dilatational and shear surface viscosity numbers are varied over a wide range. A slight dependence of all parameters on the dilatational surface viscosity and a strong dependence on the shear surface viscosity could be found.

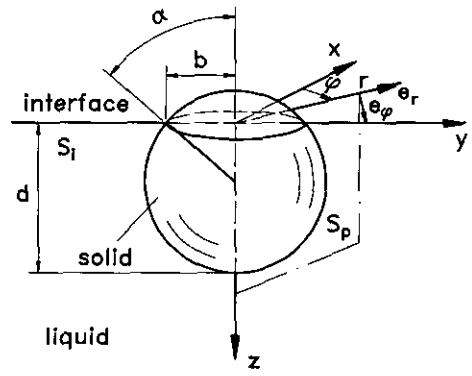

FIG. 1. Geometry of the system.

2. THEORETICAL ANALYSIS

A. Basic Equations and Boundary Conditions

We consider the stationary slow motion of a solid spherical particle partially immersed in a viscous incompressible fluid, floating on a viscous liquid–gas interface in the frame of low Reynolds number hydrodynamics. Then the pressure p and the local fluid velocity $\mathbf{v}$ obey Stokes' equations for creeping motion,

$$\nabla\cdot\mathbf{v} = 0, \quad \eta\nabla^2\mathbf{v} = \nabla p, \qquad [1]$$

where η is the dynamic viscosity and ∇ is the volume gradient. The solid spherical particle with radius a and surface S_0 performs translational motion along the Oy axis (see Fig. 1) with the characteristic velocity V. The boundary condition on the interface S_i depends on the type of the interface. For a free interface the friction is equal to zero (7, 9, 19). For a Newtonian viscous liquid interface S_i (23, 29), we consider the Boussinesq–Scriven constitutive law and define the surface-excess stress tensor $\mathbf{S}$ in the following form:

$$\mathbf{S} = \sigma\mathbf{I}_s + (\eta_d - \eta_{sh})(\nabla_s\cdot\mathbf{v}_s)\mathbf{I}_s + \eta_{sh}[(\nabla_s\mathbf{v}_s)\cdot\mathbf{I}_s + \mathbf{I}_s\cdot(\nabla_s\mathbf{v}_s)^T]. \qquad [2]$$

In [2], σ is the thermodynamical interfacial tension, η_{sh}

and η_d are, respectively, the interfacial shear and dilatational viscosity at a given point of the interface, $\mathbf{I}_s$ is the unit surface idemfactor, $\mathbf{v}_s$ is the surface velocity, and ∇_s is the surface gradient. Equation [2] is the two-dimensional analogue to the comparable expressions for the bulk-phase pressure tensor $\mathbf{P}$,

$$\mathbf{P} = -p\mathbf{I} + \eta[\nabla\mathbf{v} + (\nabla\mathbf{v})^T]. \qquad [3]$$

In [2] and [3], $(\nabla_s\mathbf{v}_s)^T$ and $(\nabla\mathbf{v})^T$ are conjugates of the tensors $(\nabla_s\mathbf{v}_s)$ and $(\nabla\mathbf{v})$, respectively. In all practical circumstances the surface-excess mass density is small compared to the bulk-phase mass density and the equation for the interfacial momentum transport reduces to the balance of the forces acting on the material interface

$$\nabla_s\cdot\mathbf{S} = \mathbf{n}_s\cdot\langle\mathbf{P}\rangle, \qquad [4]$$

where $\mathbf{n}_s$ is the unit normal to the viscous liquid interface and $\langle\mathbf{P}\rangle$ is the jump of the volume stress tensor $\mathbf{P}$. In addition we must take into account the usual kinematic boundary condition.

The resultant force $\mathbf{F}$ due to the stress exerted by the surrounding fluid on the surface of the spherical solid particle S_0 and the torque $\mathbf{M}$ experienced by the body surface are sums of the volume and interface friction

$$\mathbf{F} = \int_{S_0}\mathbf{P}\cdot\mathbf{n}dS_0 + \int_{L_0}\mathbf{S}\cdot\mathbf{l}dL_0,$$
$$\mathbf{M} = \int_{S_0}(\mathbf{r}_0\times\mathbf{P})\cdot\mathbf{n}dS_0 + \int_{L_0}(\mathbf{r}_0\times\mathbf{S})\cdot\mathbf{l}dL_0, \qquad [5]$$

where $\mathbf{r}_0$ is the position vector of a point relative to an origin at the center of the particle (Fig. 1), $\mathbf{n}$ is the vector of the running unit normal to the particle surface S_0, and $\mathbf{l}$ is the unit vector tangential to the interface and perpendicular to the particle contact line L_0. For free and viscous interfaces the boundary conditions [4] depend on the capillary number $C = \eta V/\sigma$. This number is very small for Brownian macroparticles and all our considerations below will be performed in the case for which the boundary conditions can be linearized. As shown in (20, 33), for small particles, the interface can be assumed to be a plane. For example, for glass particles with a diameter smaller than 0.05 cm the equilibrium shape of the interface is practically indistinguishable from a plane surface for all contact angles and normal water solutions. This is why we will not take into account the deformation of the interface.

B. Mathematical Model of the Problem

The system of equations [1] and boundary conditions [2]–[4] are difficult to compute directly numerically using the velocity–pressure formulation or the vorticity formulation. The difficulties connected with the specific form of the equations are discussed in (26, 27). The usual bicylindrical coordinate system (27) is not applicable for the numerical investigation of our problem because the contact line of the particle is a singularity in this coordinate system. Therefore we have transformed the problem to the equivalent well-defined system of second-order partial differential equations with known boundary conditions in a rectangular region using specific bicylindrical coordinates.

We denote $Oxyz$ as a system of Cartesian coordinates, φ a meridian angle, any plane for which φ is constant a meridian plane, and r and z, respectively, radial and vertical coordinates in a cylindrical coordinate system $Or\varphi z$ (Fig. 1). All dimensionless coordinates are introduced by scaling with the particle radius a. Let $d = 1 + \cos\alpha$ be the dimensionless immersion depth, $b = \sin\alpha$ the dimensionless contact radius, α the contact angle, and x_1 and x_2 the specific bicylindrical coordinates in the meridian planes connected with the Cartesian coordinates with the following expressions:

$$x = \frac{(1-x_2^2)b\cos\varphi}{1+2x_2\cos x_1 + x_2^2}, \quad y = \frac{(1-x_2^2)b\sin\varphi}{1+2x_2\cos x_1 + x_2^2},$$
$$z = \frac{2x_2\sin x_1 b}{1+2x_2\cos x_1 + x_2^2}. \qquad [6]$$

In this coordinate system the lines $x_1 = const$ are the circumferences

$$r^2 + (z + b\cot x_1)^2 = \frac{b^2}{\sin^2 x_1},$$

where the projection of the particle surface S_0 is the coordinate line $x_1 = -\alpha$ and the projection of the interface S_i is the coordinate line $x_1 = 0$. The lines $x_2 = const$ are the circumferences

$$z^2 + \left(r - b\frac{1+x_2^2}{1-x_2^2}\right)^2 = \frac{4b^2x_2^2}{(1-x_2^2)^2},$$

where the axis of revolution is the coordinate line $x_2 = -1$ and the contact line of the particle is transformed to the coordinate line $x_2 = 0$. The typical coordinate lines and vectors are shown in Fig. 2 for a contact angle of 45°.

After eliminating the pressure from Stokes' equations [1], one obtains a general equation for the vorticity vector $\mathbf{w}$

$$\mathbf{w} = \tfrac{1}{2}\nabla\times\mathbf{v}, \quad \nabla\times\nabla\times\mathbf{w} = \mathbf{0}. \qquad [7]$$

As outlined before, for small capillary numbers the problem has linearized boundary conditions for a floating motion. The solution of the equations contains therefore only one mode of a Fourier expansion. Hence, the dimensionless pres-

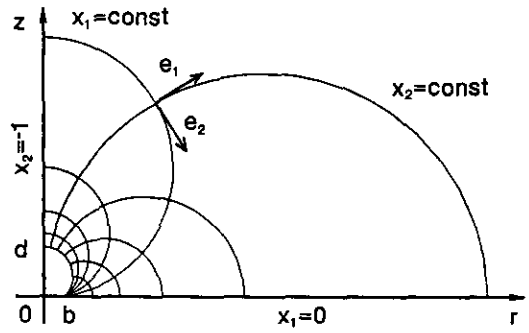

FIG. 2. Specific bicylindrical coordinates x_1 and x_2 in the plane Orz for a contact angle of 45°. The circle of radius 1, corresponding to the line $x_1 = -\alpha$, represents the projection of the particle surface, where b is the contact radius and d is the immersion depth.

sure q, the velocity, and the vorticity components in the given coordinate system can be presented in the following general form:

$$p = \frac{\eta V}{a} q \sin\varphi, \quad \mathbf{v} = V(v_1 \sin\varphi, v_2 \sin\varphi, v_\varphi \cos\varphi),$$

$$\mathbf{w} = \frac{V}{ab}(w_1 \cos\varphi, w_2 \cos\varphi, w_\varphi \sin\varphi). \quad [8]$$

The components of the velocity in the meridian plane are connected with the components of the vorticity in this plane as follows:

$$v_1 = h_1 \frac{\partial}{\partial x_1}(r v_\varphi) + \frac{2r}{b} w_2,$$

$$v_2 = h_2 \frac{\partial}{\partial x_2}(r v_\varphi) - \frac{2r}{b} w_1. \quad [9]$$

The boundary conditions [2]–[4] contain second-order derivatives of the velocity, which makes the computation of the problem a bit cumbersome. Following the two vorticity–one velocity formulation given in (26, 27), we use vorticities w_1 and w_2 and velocity v_φ. Then from [1] and [7]–[9] the equation of continuity and the partial differential equations for the components of the vorticity vector can be written in the following form:

$$\frac{\partial^2 v_\varphi}{\partial x_1^2} + x_2^2 \frac{\partial^2 v_\varphi}{\partial x_2^2} + 3A_1 \frac{\partial v_\varphi}{\partial x_1} + (3x_2A_2 + 1)x_2 \frac{\partial v_\varphi}{\partial x_2} + \frac{2}{bh_1} \frac{\partial w_2}{\partial x_1} + \frac{2}{bh_1} x_2 \frac{\partial w_1}{\partial x_2} + \frac{6A_1}{bh_1} w_2 + \frac{2x_2}{bh_1}(2A_2 - A_3)w_1 = 0$$

$$\frac{\partial^2 w_1}{\partial x_1^2} + x_2^2 \frac{\partial^2 w_1}{\partial x_2^2} + 3A_1 \frac{\partial w_1}{\partial x_1} + (x_2A_2 + 1)x_2 \frac{\partial w_1}{\partial x_2} + 2x_2A_3 \frac{\partial w_2}{\partial x_1} + B_1 w_1 + 3x_2A_1A_3 w_2 = 0,$$

$$\frac{\partial^2 w_2}{\partial x_1^2} + x_2^2 \frac{\partial^2 w_2}{\partial x_2^2} + A_1 \frac{\partial w_2}{\partial x_1} + (3x_2A_2 + 1)x_2 \frac{\partial w_2}{\partial x_2} + B_2 w_2 - 2x_2(A_2 + A_3) \frac{\partial w_1}{\partial x_1} - 2x_2A_1 \frac{\partial w_1}{\partial x_2} - x_2A_1(A_3 + 4A_2)w_1 = 0. \quad [10]$$

Let us transform the boundary conditions of the problem for the defined functions. For a solid spherical particle floating with constant relative translational velocity in Oy direction the no-slip condition on the particle surface gives the boundary condition for the dimensionless meridian velocity component and from [9] we can obtain the Dirichlet boundary condition for the dimensionless vorticity components at the surface S_0. At infinity the values of the two vorticities w_1 and w_2 and the velocity v_φ go to zero. For all types of interfaces (free and viscous) the linearized kinematic boundary condition (the normal component of the velocity is equal to zero) from [9] reduces to the Dirichlet boundary condition for w_2 for a given value of v_φ. For a free interface, the friction is negligible and the normal derivatives of the meridian component of the velocity and the first component of the vorticity are equal to zero on it. For a viscous interface the tangential components of the linearized stress boundary condition [2]–[4] using the definitions [8]–[9] and Eq. [10] can be reduced to the following system of second-order partial differential equations for the velocity component v_φ and vorticity component w_1 at the interface $x_1 = 0$:

$$\frac{\partial v_\varphi}{\partial x_1} = (K + E)h_1 \times \left[x_2^2 \frac{\partial^2 v_\varphi}{\partial x_2^2} + x_2(x_2A_3 + 3x_2A_2 + 1) \frac{\partial v_\varphi}{\partial x_2} \right] + \frac{2K}{b} x_2 \frac{\partial w_1}{\partial x_2} + 4(K + E) \frac{x_2A_2}{b} w_1,$$

$$\frac{\partial w_1}{\partial x_1} + x_2A_3 w_2 = Eh_1 \left[x_2^2 \frac{\partial^2 w_1}{\partial x_2^2} + x_2(x_2A_2 + x_2A_3 + 1) \frac{\partial w_1}{\partial x_2} - \frac{4x_2^2}{(1 - x_2^2)^2} w_1 \right], \quad [11]$$

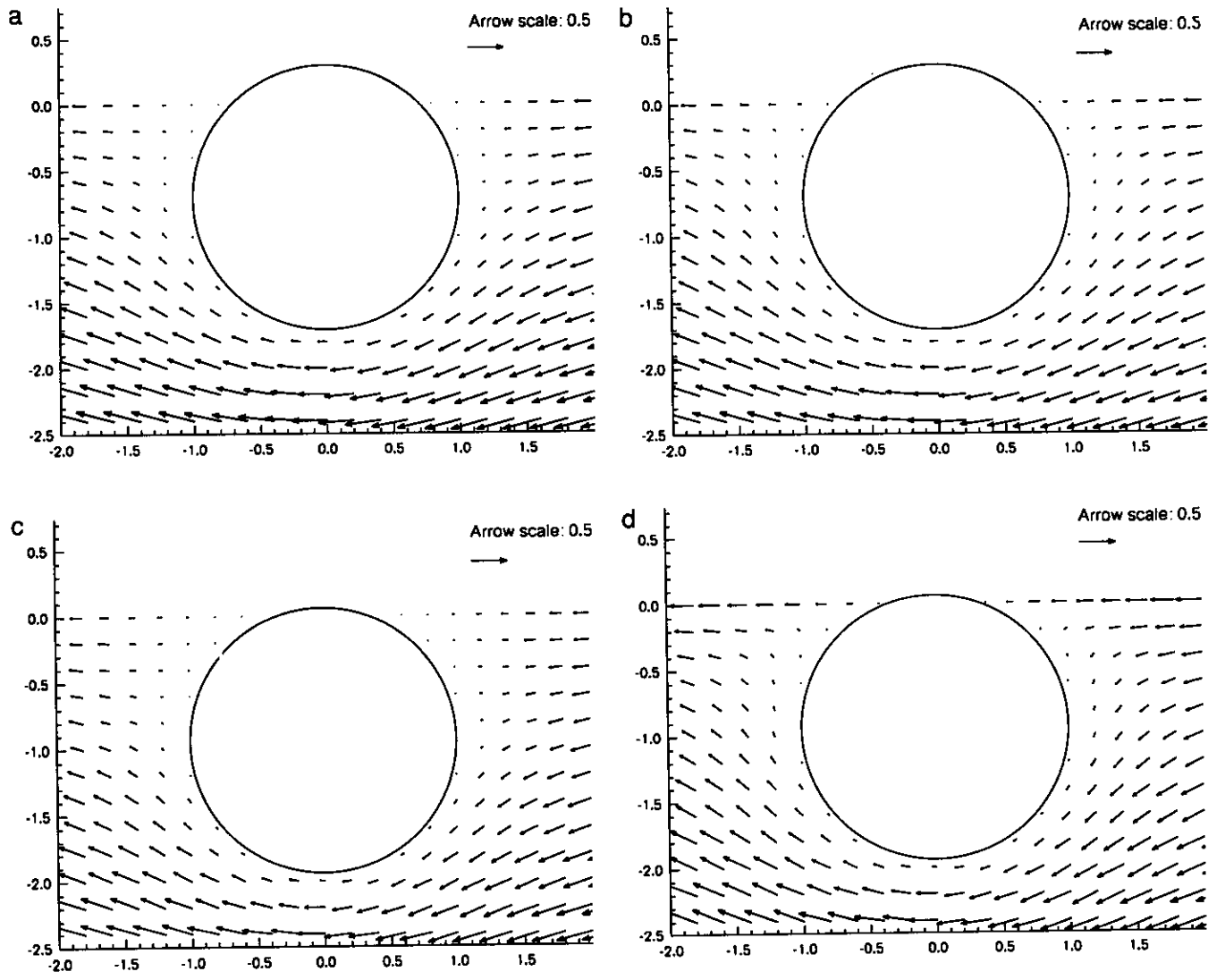

FIG. 3. Velocity field in the plane $x = 0$ for contact angles of (a, b) 45° and 20° (c, d); (a, c) free interface, (b, d) $K = E = 10$.

where $K = \eta_d/\eta a$ and $E = \eta_{sh}/\eta a$ are the dilatational and the shear surface viscosity number, respectively. In the case of very small surface viscosity numbers one can obtain from [11] similar solutions for the free interface. From [10] the asymptotic behavior of the meridian component of the velocity and the components of the vorticity on the axis of revolution ($x_2 = -1$) defines the boundary condition: the first derivative of v_φ and w_2 normal to the axis and the vorticity component w_1 are equal to zero. From an asymptotic analysis of Eq. [10] one can derive the following boundary conditions on the contact line at $x_2 = 0$:

$$v_\varphi = 1, \quad w_1 = \frac{1}{4b}\sin(x_1 + \alpha)\frac{\partial v_\varphi}{\partial x_2},$$

$$w_2 = \frac{1}{4b}\cos(x_1 + \alpha)\frac{\partial v_\varphi}{\partial x_2}. \qquad [12]$$

In Eqs. [9]–[11] the metrical functions and other coefficients are known functions of the coordinates defined by

$$A_1 = \frac{2x_2\sin x_1}{1 + 2x_2\cos x_1 + x_2^2},$$

$$A_2 = -\frac{2[2x_2 + (1 + x_2^2)\cos x_1]}{(1 - x_2^2)(1 + 2x_2\cos x_1 + x_2^2)},$$

$$A_3 = -\frac{1 - x_2^2}{x_2(1 + 2x_2\cos x_1 + x_2^2)},$$

$$B_1 = A_1^2 - x_2^2A_2^2 - x_2^2A_3^2, \quad B_2 = -1 - 3A_1^2,$$

$$h_1 = -\frac{1}{2bx_2}(1 + 2x_2\cos x_1 + x_2^2),$$

$$h_2 = \frac{1}{2b}(1 + 2x_2\cos x_1 + x_2^2).$$

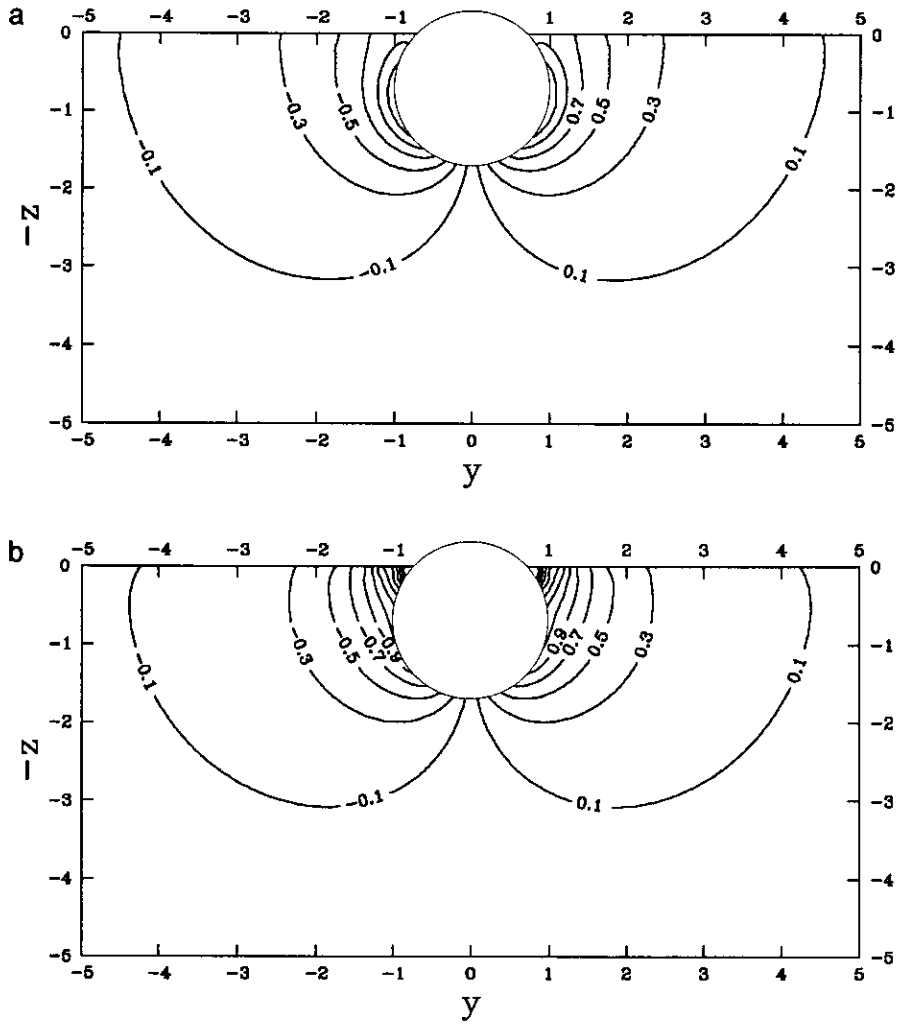

FIG. 4. Pressure distribution in the plane $x = 0$ for a contact angle of 45° in the cases: (a) free interface, (b) $K = E = 10$.

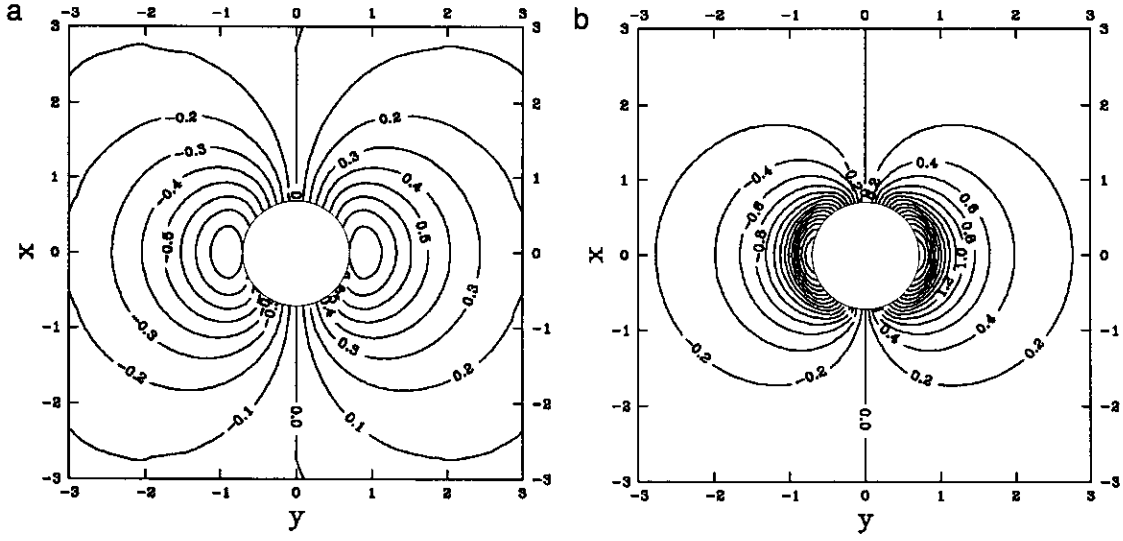

FIG. 5. Pressure distribution on the interface for a contact angle of 45° in the cases: (a) free interface, (b) $K = E = 10$.

Using the definitions [8] and [9], one can compute the physical components of the velocity and the pressure distribution using the meridian plane of Stokes' equation.

After a detailed analysis of [2], [3], and [5], we proved that in our case only the y component of the drag force and the x component of the torque exerted by the surrounding fluid were nonzero. The general form of them is

$$F_y = f\pi\eta aV, \quad M_x = m\pi\eta a^2 V, \qquad [13]$$

where the dimensionless drag coefficient f and the dimensionless torque coefficient m are evaluated by the following solutions:

$$f = f_{sv} + \int_{-1}^{0} \left\{ -r\frac{h_1}{h_2}\frac{\partial r}{\partial x_1} q + r\frac{h_1}{h_2}\frac{\partial v_\varphi}{\partial x_1} + rh_1\frac{\partial r}{\partial x_2}\frac{\partial v_2}{\partial x_1} \right\} dx_2,$$

$$m = m_{sv} - \int_{-1}^{0} \left(r\frac{h_1}{h_2}\frac{\partial v_2}{\partial x_1} + rh_1\frac{\partial r}{\partial x_2}\frac{\partial v_\varphi}{\partial x_1} \right) dx_2. \qquad [14]$$

In [14] the additional interface drag and torque coefficients f_{sv} and m_{sv} are equal to zero for a free interface and for a viscous interface they can be evaluated from the following solutions:

$$f_{sv} = bE\frac{\partial v_\varphi}{\partial r} + b(K+E)\frac{\partial v_r}{\partial r},$$

$$m_{sv} = -f_{sv}\cos\alpha \text{ at } x_1 = 0,\ x_2 = 0. \qquad [15]$$

The normal component of the linearized stress boundary condition [2]–[4] gives the equation for the first Fourier mode deviation of the shape S_i. The disturbances of the surface shape are proportional to the capillary number C and in our cases the effect of the deformation of the interface is of second-order. For our numerical computation of the equations we used the modified alternating direction implicit method proposed in (26) for a similar problem, a moving particle in a viscous liquid layer, which gives the possibility to compute with second-order implicit time- and space-variable interpolation.

3. NUMERICAL RESULTS AND DISCUSSIONS

A. *Velocity and Pressure Distribution*

In order to illustrate the influence of the surface viscosity on the overall velocity and pressure distribution, we computed the flow field for a particle floating on the interface for two different contact angles. The particle is moving in Oy-direction with velocity 1. However, as the effects in the vicinity of the particle are difficult to interpret, we plotted the velocity field of the fluid relative to the particle, i.e., $v - 1$. In Fig. 3 the velocity field in the vicinity of the particle is shown for four different cases: (a) a free interface ($K = E = 0$), $\alpha = 45°$; (b) a highly viscous interface ($K = E = 10$), $\alpha = 45°$; (c) $K = E = 0$, $\alpha = 20°$; and (d) $K = E = 10$, $\alpha = 20°$. One can see that the size of the stagnation area in front and behind the floating particle close to the interface increases with increasing surface viscosity. The size of the stagnation area does not strongly depend on the contact angle. At $\alpha = 20°$ it is of course larger than at $\alpha = 45°$ and it vanishes as the contact angle tends to 90°.

In Figs. 4a and 4b we plotted the isobars corresponding to the velocity fields of Figs. 3a and 3b. Here the effects are more pronounced and therefore easier to understand. The isobars denoted with 0.3 and 0.5 are hardly distinguishable in both plots, but one can clearly see how the fluid gets "caught" between the interface and the particle surface for the case of high viscous interface (see Fig. 4b). The location of the stagnation point also depends on the surface viscosity as well as on the contact angle. For a contact angle of 90°, it is on the three-phase contact line but for smaller contact angles it moves in positive Oz direction when the surface viscosity drops. In order to demonstrate the three-dimensional character of the problem, the pressure distribution on the interface for the same conditions as in Figs. 3a and 3b are shown in Figs. 5a and 5b. The pressure distribution on the interface is antisymmetric to the plane $y = 0$, as can be seen from Eq. [8].

B. *Drag and Torque Coefficients*

With sufficient insight into the characteristic features of the flow field, one can understand the effects governing the behavior of the drag and torque coefficients. In Fig. 6a the drag coefficient is shown as a function of the contact angle for four different surface viscosity numbers: (1) $K = E = 0$, (2) $K = E = 1$, (3) $K = E = 5$, (4) $K = E = 10$. For a free surface (curve 1), the absolute value of the drag coefficient at a contact angle of 90° is exactly 3, corresponding to 50% of the value of Stokes' solution for a particle moving in an unbounded fluid. However, decreasing the contact angle down to 20° leads to an increase of the drag force of almost 50%. In contrast, for high surface viscosity (curves 3 and 4) the drag coefficient is almost independent of the contact angle. This is due to the fact that in this case the hydrodynamic resistance is determined by the stagnation area which for viscous interfaces is almost as large for high contact angles as for lower ones.

The torque coefficient presented in Fig. 6b for the same conditions as in Fig. 6a is not very sensitive to changes of the contact angle for low values of K and E. In this case the torque is determined by the friction between the lower half of the sphere and the surrounding fluid. Decreasing the contact angle only slightly decreases the torque, because of the stagnation zone covering the additional surface of the particle which is in contact with the fluid. For interfaces with high values of surface viscosity numbers (curves 3 and

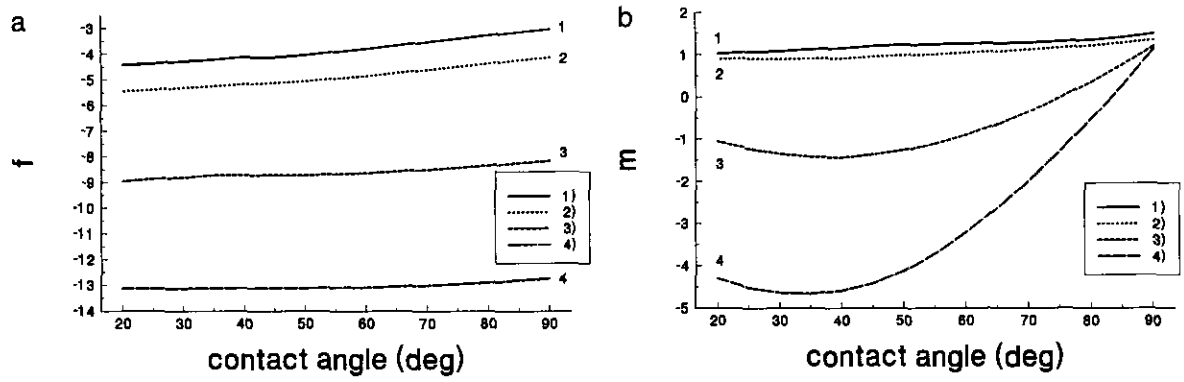

FIG. 6. Dependence of (a) the drag coefficient and (b) the torque coefficient on the contact angle: (1) free interface, (2) $K = E = 1$, (3) $K = E = 5$, (4) $K = E = 10$.

4), a considerable influence of the contact angle on the torque coefficient could be found. At 90° the friction force exerted by the viscous interface on the particle acts directly toward the center of the sphere. Hence, the torque coefficient is almost the same as for a low viscous interface. For lower contact angles the force of the viscous interface results in a remarkable torque, acting in opposite direction to the friction force of the bulk fluid. In fact, the effect caused by the interface is so strong that the torque coefficient changes its sign and consequently, the particle rotates in the opposite direction. When the particle is further immersed into the fluid, the absolute value of the torque coefficient decreases again, which appears reasonable when compared to the case of a sphere moving close to a viscous interface considered in (27).

A better understanding of the dependence of the drag and torque coefficient on the surface viscosity numbers can be gained from Figs. 7a and 7b, where the four curves represent different contact angles: (1) 30°, (2) 50°, (3) 70°, and (4) 90°. For all cases the drag coefficient shows an almost linear drop when the surface viscosity increases with a stronger influence of the contact angle at low values of K and E than at higher values. In contrast, the torque coefficient remains almost constant until a critical value of the surface viscosity numbers about 1, from which a similar linear dependence on the surface viscosity can be perceived.

For most practically important cases, the dilatational and the shear surface viscosity number are of the same order of magnitude. Only in extreme cases, such as some biological membranes, can they differ by several orders of magnitude. However, it is quite common that they differ by a factor from 0.2 to 5 and therefore we investigated the individual effects of the different types of viscosity. In Fig. 8 we plot the drag coefficient as a function of the shear surface viscosity number for three different contact angles: (a) 20°, (b) 60°, and (c) 80°. In addition, four curves for different dilatational surface viscosities are presented in each plot: (1) $K = 0$, (2) $K = 1$, (3) $K = 5$, and (4) $K = 10$. It becomes quite clear that the linear drop perceived in Fig. 7a is almost only due to the influence of the shear surface viscosity. This is an important result of our analysis for a partially immersed particle, as in (29) it was proved that for a viscous droplet moving in an unbounded fluid the motion is only influenced by the dilatational surface viscosity. The effects of the individual viscosities having been singled out, Fig. 8 represents a powerful tool to determine the dilatational surface viscosity in ranges where the surface shear viscosity is known through measurements of the drag coefficient of a floating particle.

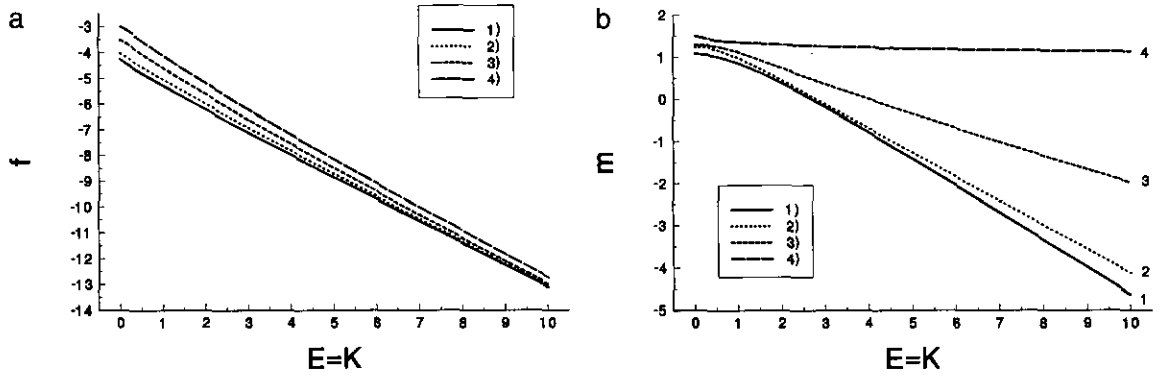

FIG. 7. Dependence of (a) the drag coefficient and (b) the torque coefficient on the surface viscosity number $K = E$: (1) $\alpha = 30°$, (2) $\alpha = 50°$, (3) $\alpha = 70°$, (4) $\alpha = 90°$.

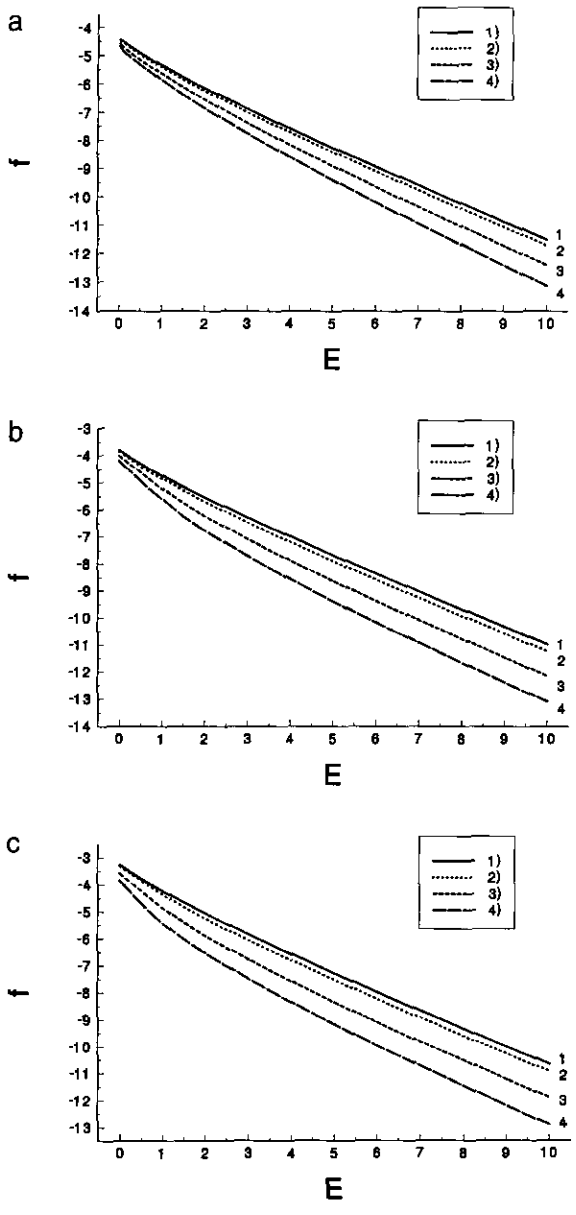

FIG. 8. Dependence of the drag coefficient on the shear surface viscosity number for contact angles of (a) 20°, (b) 60°, and (c) 80°: (1) $K = 0$, (2) $K = 1$, (3) $K = 5$, (4) $K = 10$.

For many practically relevant cases, this might be easier than the maximum bubble pressure method (see (35) and (36)). In addition, it is known that for $\eta_{sh} < 1$ sp the dilatational viscosity has no influence on the particle motion. Therefore, from measured drag coefficients we can also determine shear viscosities of the order of 0.001 sp. It would be interesting to compare such results to measured values gained with a knife-edge surface viscosimeter (see, e.g., (34)).

C. The Surface Diffusion Coefficient

Considering the drag-out problem for certain applications where particles float on the surface of the liquid or are dip-coated, quantitative information on the surface diffusion coefficient might be of considerable practical importance. Following (5–9) the surface diffusion coefficient D_s of a particle floating on a viscous interface in the frame of Einstein's theory can be written in the form

$$D_s = \frac{kT}{f\pi\eta a}, \qquad [16]$$

where k is Boltzmann's constant and T is the temperature. In Fig. 9 we plot the ratio of this surface diffusion coefficient relative to the surface diffusion coefficient D_{s0} for a free interface. The curves in Fig. 9a represent different values of the surface viscosity numbers: (1) $K = E = 1$, (2) $K = E = 5$, (3) $K = E = 10$. The absolute value of D_s is of course smaller for smaller contact angles than for large values of α. However, the slope of the curves indicates that the mobility of a particle on a viscous surface changes less significantly with the contact angle than the mobility of a particle floating on a free interface. In addition, one can see that the relative change of the surface diffusion coefficient is more pronounced for contact angles larger than 45° than for smaller values. Figure 9b gives a better impression of the dependence of the relative surface diffusion coefficient on the surface viscosity numbers for four different contact angles: (1) 30°, (2) 50°, (3) 70°, and (4) 90°. Apparently, the most important decrease of the mobility of the floating particle takes place in the range $0 < K, E < 5$, with a less significant drop for higher values of K and E.

4. CONCLUSIONS

The model presented for computing drag, torque, and surface diffusion coefficients makes it possible to investigate the influence of the surface viscosity on the motion, the hydrodynamic resistance, and the surface diffusivity of the large Brownian particle floating on the viscous interface. It can be used for small Reynolds and capillary numbers and a linear Newtonian viscous interface model when the weight of the particle is not high enough to cause a deformation of the interface.

Our calculations revealed that the drag and torque exerted on a floating particle depend heavily on the surface viscosity as well as on the contact angle. In particular we could prove that for contact angles of less than 90°, the particle can be forced to rotate in different directions when traveling along the surface, depending on the surface viscosity number. The information provided for the dependence of the drag coefficient on the shear and dilatational surface viscosity number, respectively, can be utilized to determine the dilatational surface viscosity when the shear viscosity number is known. Moreover, when the shear surface viscosity is much smaller than 1 sp and hence the influence of the dilatational surface viscosity vanishes, our calculations can also be used to deter-

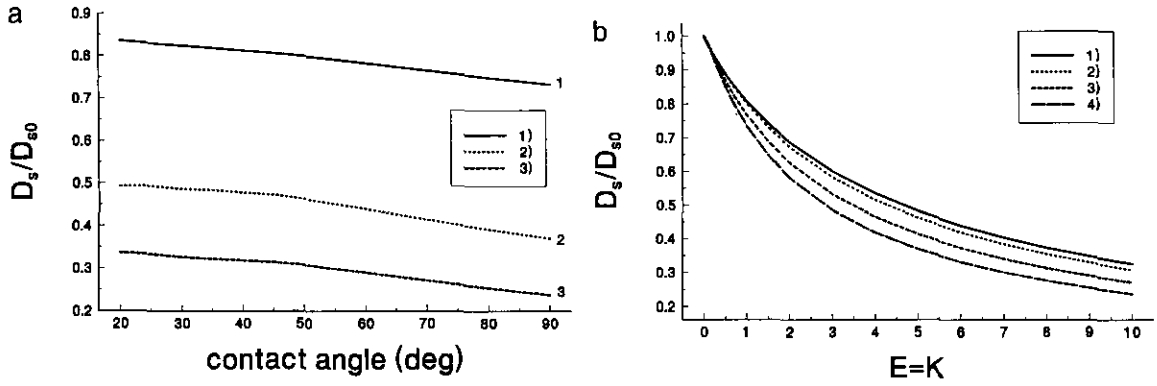

FIG. 9. (a) Dependence of the ratio of the surface diffusion coefficient D_s and the free surface diffusion coefficient D_{s0} on the contact angle: (1) free interface, (2) $K = E = 1$, (3) $K = E = 5$, (4) $K = E = 10$. (b) Dependence of the ratio of the surface diffusion coefficient D_s and the free surface diffusion coefficient D_{s0} on the surface viscosity number $K = E$: (1) $\alpha = 30°$, (2) $\alpha = 50°$, (3) $\alpha = 70°$, (4) $\alpha = 90°$.

mine the shear surface viscosity from measurements of the drag force coefficient.

Finally, our calculations of the surface diffusion coefficient provide useful background information for the drag-out problem with particles or certain cases of dip coating.

ACKNOWLEDGMENTS

The authors thank Professor Ivan B. Ivanov and Dr. Hans Raszillier for their most helpful discussions. This research was supported financially by "Volkswagen-Stiftung." The authors gratefully acknowledge this support of their collaborative research.

REFERENCES

1. Einstein, A., *Ann. Phys.* **19,** 289 (1906).
2. Kubo, R., *Rep. Prog. Phys.* **29,** 255 (1966).
3. Davis, R. H., *Adv. Colloid Interface Sci.* **43,** 17 (1993).
4. Russel, W. B., Saville, D. A., and Schowalter, W. R., "Colloid Dispersions." Cambridge Univ. Press, Cambridge, UK, 1989.
5. Brenner, H., and Leal, L. G., *J. Colloid Interface Sci.* **65,** 191 (1978).
6. Brenner, H., and Leal, L. G., *J. Colloid Interface Sci.* **88,** 136 (1982).
7. Radoev, B., Nedjalkov, M., and Djakovich, V., *Langmuir* **8,** 2962 (1992).
8. Dimitrov, K., Radoev, B., and Avramov, M., *Langmuir* **9,** 1414 (1993).
9. Mileva, E., and Nikolov, L., *J. Colloid Interface Sci.* **161,** 63 (1993).
10. Feng, S.-S., *J. Colloid Interface Sci.* **160,** 449 (1993).
11. Faxén, H., Dissertation, Uppsala University, 1921.
12. Happel, J., and Brenner, H., "Low Reynolds Number Hydrodynamics with Special Applications to Particulate Media," Prentice Hall, Englewood Cliffs, NJ, 1965.
13. Hetsroni, G., "Handbook of Multiphase System" (G. Hetsroni, Ed.). Hemisphere, Washington, DC, 1982.
14. Dean, W. R., and O'Neill, M. E., *Mathematika* **10,** 13 (1963).
15. O'Neill, M. E., *Mathematika* **11,** 67 (1964).
16. O'Neill, M. E., and Stewartson, K., *J. Fluid Mech.* **27,** 705 (1967).
17. Goldman, A. J., Cox, R. G., and Brenner, H., *Chem. Eng. Sci.* **22,** 637 (1967).
18. Cooley, M. D. A., and O'Neill, M. E., *J. Inst. Math. Appl.* **4,** 163 (1968).
19. Yang, S.-M., and Leal, L. G., *Int. J. Multiphase Flow* **16,** 597 (1990).
20. Stoos, J. A., and Leal, L. G., *J. Fluid Mech.* **217,** 263 (1990).
21. Boussinesq, M. J., *Ann. Chim. Phys.* **29,** 349 (1913).
22. Sternling, C. V., and Scriven, L. E., *AIChE J.* **5,** 514 (1959).
23. Scriven, L. E., *Chem. Eng. Sci.* **12,** 98 (1960).
24. Zapryanov, Z., Malhotra, A. K., Aderangi, N., and Wasan, D. T., *Int. J. Multiphase Flow* **9,** 105 (1983).
25. Malhotra, A. K., and Wasan, D., *Chem. Eng. Commun.* **55,** 95 (1987).
26. Danov, K. D., Aust, R., Durst, F., and Lange, U., submitted for publication.
27. Danov, K. D., Aust, R., Durst, F., and Lange, U., submitted for publication.
28. Levich, V. G., "Physicochemical Hydrodynamics." Prentice Hall, Englewood Cliffs, NJ, 1962.
29. Edwards, D. A., Brenner, H., and Wasan, D., "Interfacial Transport Processes and Rheology." Butterworth–Heinemann, Boston, 1991.
30. Hunter, R. J., "Foundation of Colloid Science," Vol. I. Clarendon, Oxford, 1987.
31. Hunter, R. J., "Foundation of Colloid Science," Vol. II. Clarendon, Oxford, 1989.
32. Kim, S., and Karrila, S. J., "Microhydrodynamics: Principles and Selected Applications." Butterworth–Heinemann, Boston, 1991.
33. Princen, H. M., *in* "Surface and Colloid Science" (E. Matijevic and F. R. Eirich, Eds.), Vol. 2, p. 1. Wiley, New York, 1969.
34. Goodrich, F. C., Allen, L. H., and Poskanzer, A., *J. Colloid Interface Sci.* **52,** 201 (1975).
35. Kao, R. L., Edwards, D. A., Wasan, D. T., and Chen, E., *J. Colloid Interface Sci.* **148,** 247 (1992).
36. Kao, R. L., Edwards, D. A., Wasan, D. T., and Chen, E., *J. Colloid Interface Sci.* **148,** 257 (1992).
37. Schneider, J. C., O'Neill, M. E., and Brenner, H., *Mathematika* **20,** 175 (1973).
38. Majumdar, S. R., O'Neill, M. E., and Brenner, H., *Mathematika* **21,** 147 (1974).
39. Kunesh, J. G., Brenner, H., O'Neill, M. E., and Falade, A., *J. Fluid Mech.* **154,** 29 (1985).
40. O'Neill, M. E., Ranger, K. B., and Brenner, H., *Phys. Fluids* **29,** 913 (1986).